January 1995

Global asymptotic stability of a passive juggling strategy: A possible parts-feeding method

P. J. Swanson
University of Michigan

Robert R. Burridge
University of Michigan

Daniel E. Koditschek
University of Pennsylvania, kod@seas.upenn.edu

Reprinted from *Mathematical Problems in Engineering*, Volume 1, Issue 3, 1995, pages 193-224.
Publisher URL: http://dx.doi.org/10.1155/S1024123X95000135

Global asymptotic stability of a passive juggling strategy: A possible parts-feeding method

Abstract
In this paper we demonstrate that a passive vibration strategy can bring a one-degree-of-freedom ball to a specified periodic trajectory from all initial conditions. We draw motivation from the problem of parts feeding in sensorless assembly. We provide simulation results suggesting the relevance of our analysis to the parts feeding problem.

Keywords
factory automation, robotics, chaotic dynamics, parts feeding, parts feeders, vibration

Comments
Reprinted from *Mathematical Problems in Engineering*, Volume 1, Issue 3, 1995, pages 193-224.
Publisher URL: http://dx.doi.org/10.1155/S1024123X95000135

MPE — Volume 1, pp. 193-224
Reprints available directly from the publisher
Photocopying permitted by license only

GLOBAL ASYMPTOTIC STABILITY OF A PASSIVE JUGGLING STRATEGY: A POSSIBLE PARTS-FEEDING METHOD*

P. J. SWANSON, R. R. BURRIDGE, and D. E. KODITSCHEK

Artificial Intelligence Laboratory, EECS Department, College of Engineering, University of Michigan, Ann Arbor MI 48105-2110.

In this paper we demonstrate that a passive vibration strategy can bring a one-degree-of-freedom ball to a specified periodic trajectory from all initial conditions. We draw motivation from the problem of parts feeding in sensorless assembly. We provide simulation results suggesting the relevance of our analysis to the parts feeding problem.

AMS Nos.: 58 Global analysis, analysis on manifolds; 70 Mechanics of particles and systems: 93 Systems theory; control
Keywords: Factory automation; robotics; chaotic dynamics; parts feeding; parts feeders; vibration

1. INTRODUCTION

As industry moves toward faster product cycles, smaller production runs, and shorter product development time, the idea of flexible manufacturing as a means of improving the quality, variety, and overhead cost of producing goods has caught on. Programmable mechanisms—robots, NC controlled milling machines, and so on—abound. However, much of this machinery suffers from a common drawback: parts need to be fed, one at a time and, absent sensors, each part must be fed in a precise orientation at a precise location. This is the Parts Feeding Problem, which has been the subject of considerable academic interest [5, 10] and industrial concern [2]. "Ultimately, the smartest assembly robot and the best assembly machine in the world are useless without the mechanism that delivers the parts [12]."

1.1. Parts Feeding: The Orientation Problem

The Parts Feeding Problem can be broken into three subproblems: *singulation*, *orientation*, and *presentation*. Singulation is the process of separating the mass of parts into individual parts, and can be very difficult if the parts nest within each other easily (like thimbles) or become entangled (like paper clips). Orientation is the process of reorienting the randomly oriented parts to a small predetermined subset of the possible orientations (typically only one). Presentation is the action of moving the singulated and oriented part to a known location, where a machine tool or robot can easily perform an operation on it.

*This work was supported, in part, by the NSF under grant IRI-9123266, and in part by Deneb Robotics, Inc. The third author gratefully acknowledges the hospitality of the Japan MITI Mechanical Engineering Laboratory where he began the initial work on this project.

The problem of singulation is unique to each family of similar parts. No automated technique of performing singulation for an arbitrary part exists, so singulation strategies are often custom designed through trial and error for each new type of part. Failures in singulation strategies are often not discovered until the factory is ready to start production, since there is also no automated way of determining whether two parts will become tangled again down line from the singulation process [27]. Current flexible parts feeding strategies assume that the parts are pre-singulated and concentrate on the orientation step.

The orientation problem lies at the heart of the parts feeding problem. Little is known about how to orient an arbitrary part beyond decades of craftsmanship and experience. Even in textbooks, the orientation problem is presented with a cookbook approach, in the manner of "this approach worked with this type of part [5, 4, 10, 18]."

Once a part is singulated and oriented, it still must be presented to the machinery. This is the easiest part of the parts feeding problem, usually accomplished with a conveyor or buffer.

1.2. Current Technology

Often, the parts that need to be fed are manufactured in a known orientation. If this orientation could be maintained throughout the assembly process, there would be little need for a parts feeder. However, for many inexpensive parts it is not economical to maintain orientation. Such parts are typically shipped or stored in bins, and are oriented only when necessary for feeding.

Current technology in parts feeders relies heavily on rejection techniques. These techniques randomize the orientation of the parts, often by shaking or dropping them, and then reject all those parts which are not in the correct orientation. The rejected parts are then recirculated, and the process repeats indefinitely. Rejection-based feeders include vibratory bowls, centrifugal disks, and various conveyor-based approaches. Custom tooling for these feeders often makes them expensive and inflexible. Research into the probability distribution of stable random part orientations [33] suggests that for a typical part, a minority[1] of the parts will randomly assume the correct orientation. For this reason, rejection based methods are very inefficient [6].

Vision-based systems replace the obstacles in the conveyor approach, requiring a robot manipulator to separate the good and bad orientations. A camera records the image of parts, and is capable of determining the position, two-dimensional orientation and, to a limited degree, shape of each part in its field of vision. A robot then removes the properly oriented parts, and the rest are recirculated. The robot may also partially reorient parts at the expense of cycle time. The major problems of vision systems include lighting difficulties [9], processing speed, and robot cycle time. The result is that vision systems have an advantage in flexibility over hard-tooled feeders, at the expense of a much slower feed rate.

[1]We note that flat or round parts have a high probability of randomly assuming a useful orientation, and are easily fed with existing technology. We consider here more complex parts, such as irregular polyhedra.

1.3. Contributions and Background

We present preliminary simulation results from a three-degrees-of-freedom simplification of the parts-feeding problem, and analysis of a system which is a one-degree-of-freedom further simplification of this problem. We hope this suggestive analysis will lead to more general results which may ultimately be useful for industrial parts-feeding applications. Section 2 states the general problem and develops the simplified setting. Section 3 presents an analysis of that setting. Section 4 derives our formal results.

Mason and colleagues have pioneered the analysis and potential assembly applications of sensorless manipulation in the robotics field [11]. Canny and Goldberg have enlarged and have begun to formalize this program in the effort to minimize sensing and automation complexity without unduly compromising its usefulness [8]. An interesting and rather different approach to the parts-feeding problem considered here has recently been taken by Böhringer and colleagues [3], who consider the possibility of reorienting planar parts through nodal shapes introduced by plate vibrations in the supporting table. Antecedent to this work, Singer and Seering [26] investigated the problem of parts rocking (rather than bouncing) on a vertically vibrating table. Sony's APOS system [25] nests multiple parts on a vibrating tray with indentations shaped to conform to the desired pose. Grossman and Blasgen's tilted vibrating box randomized motion, capturing parts in a limited number of predictable poses, which could be distinguished by simple probe measurements [13].

We seek in this paper to enlist properties of dynamical manipulation in the program of reduced sensory and actuator complexity just described. We adapt suggestive work by Atkeson and Schaal on the "Shannon juggler" to the sensorless manipulation paradigm [23]. The robotics literature reports a growing number of experimental successes with dynamical manipulation, mostly involving hopping, walking, or juggling mechanisms [1,7,17,20,21,26].

Analysis of these machines has also been reported, albeit with more limited success [15, 30, 35]. There is a large and growing analytical literature surrounding the one-degree-of-freedom bouncing ball that we study here, most of it motivated by an interest in chaos [14, 28]. We, of course, are interested in stable motion.

In this paper we analytically demonstrate the feasibility of deterministically manipulating the stable dynamic behavior of a one-degree-of-freedom part without the use of feedback. This is equivalent to juggling without sensing.

2. PROBLEM STATEMENT

Since rejection techniques are inefficient, and remote sensing and orientation techniques are often slow or expensive, we examine a potentially alternative strategy. Namely, we seek to design a table motion which will cause all the "bodies" on the table to asymptotically approach a known state without using feedback. We propose a flat, level, three-degree-of-freedom vibratory table as a viable means of orienting pre-singulated parts.

The vibrational strategy should work by bouncing parts gently on the table vertically, while inducing momentary horizontal forces at the contact points which cause a torque to be applied to the center of mass. One would hope that, if the vibrations are adequately designed, after a short period of time the parts will all rotate to a stationary predetermined

orientation. The shaking may then be stopped and the parts would land in this known orientation. Different part geometries and material properties ought to require different vibration strategies. But changing the type of part should only require changing the vibration strategy in software: the lack of orienting devices mounted on the table should allow a wide range of parts to be oriented without changing the hardware.[2]

The problem now amounts to finding favorable vibration parameters—wave shape, frequency, magnitude—or, indeed, determining whether such parameters exist at all. Despite the intuitively compelling nature of this idea, it turns out that the design of such vibratory strategies seems possible but not obvious, as our preliminary simulation data will suggest.

In this preliminary study, we consider only impacts between the table and a single part. Neither the three-degree-of-freedom simulation model nor the one-degree-of-freedom analytical model presented in this paper allow for the possibility of two flying parts knocking against each other. While this is evidently an unrealistic simplification, we prefer to explore the single-part-orientation problem before embarking on the much more complicated multiple-part problem. Moreover, to begin our investigation, we have elected to work in a deterministic framework with the emphasis on a global result. We hope (but, of course, have as yet no reason to claim) that vibration strategies inducing a large domain of attraction in the deterministic single-part setting will translate into a very high probability of orientation in the multiple-part, real-world setting.

2.1. General Problem and Successive Simplifications

Figure 1 depicts a three-degree-of-freedom simplification of the general problem. In this simplification, the part is free to move in the x, y, and θ directions, while the table follows a preprogrammed motion in the x and y directions. Several assumptions make the simulation more tractable. The coefficients of restitution and friction are assumed to be constant when, in reality, these values are often unpredictable during impulsive interactions. The table is assumed to have very large mass compared with the part, so that the impacts of the part on the table do not affect the table motion. It is assumed that the part does not lose energy while in flight. The restriction to one rotational degree of freedom eliminates complications resulting from several axes of rotation. Furthermore, it is assumed that the stick, slip, and reverse-slip dynamics caused by the rotation of the part as it contacts the table are governed by the rules developed by Routh [22] and refined by Wang [31]. In the face of this long list of assumptions, we view the simulation results as merely suggestive. We are presently developing an experimental apparatus to test the validity of this model.

Figure 2 depicts a typical simulation of the part–table interaction shown in Figure 1. In this simulation, the parts are constrained to move in vertical planes indicated by the horizontal lines on the table. The simulation uses a standard three-degree-of-freedom Newtonian flight model when the part is not in contact with the table, and employs an impact model developed by Wang and Mason [32] as soon as a contact is made. As

[2]The three degrees-of-freedom of the table are each translational: rotational motion of the table is not allowed, because the parts near the edges of the table would experience different forces than those in the center.

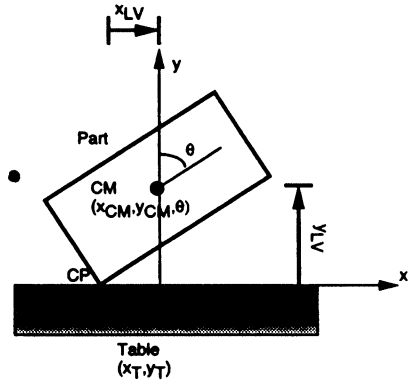

Figure 1 A three-degree-of-freedom model of the part-orientation problem.

mentioned above, each part is integrated in isolation from all the others: part–part interactions are not modeled. Each part was modeled as a 1- × 2- × 4-cm block of aluminum. The foremost row of parts on the table have initial orientations θ_0 at $t = 0$ from $\theta_0 = 0°$ to $\theta_0 = 9°$, viewed from left to right. Each successive row on the table increases the initial orientation by 10°, up to the lone part in the back row with $\theta_0 = 90°$. All parts are initially in contact with the table in their lowest corners. Letting the parts fall in gravity without vibration, those with orientations 0–26° are attracted to the 0° orientation, while those with orientations 27–90° are attracted to the 90° orientation.

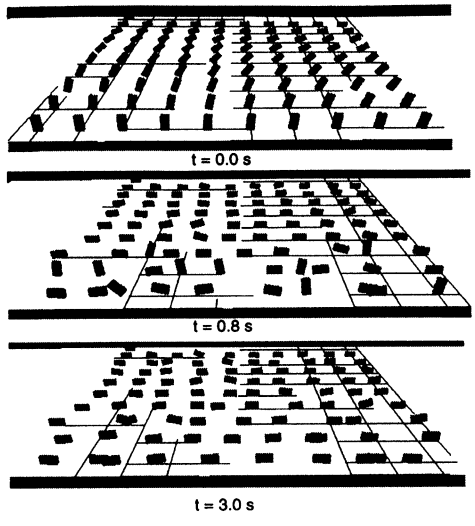

Figure 2 The three-degree-of-freedom simulation. Parts are constrained to move in vertical planes indicated by horizontal lines on the table. Part–part interactions are not modeled. In the top scene, 91 initial conditions of a part are shown in parallel laminar plates. Their evolution after 0.8 and 3.0 seconds is depicted in the two lower scenes. For this particular run, the table vibration was 60 Hz 0.2 mm in the y direction in phase with 30 Hz 1.0 mm in the x direction.

Figure 2 now depicts the future evolution of these 91 different initial conditions at times $t = 0$ *s*, $t = 0.8$ *s*, and $t = 3.0$ *s* in the face of a table vibration. For this particular run, the table vibration was a 60 Hz 0.2 mm sinusoidal vibration in the y direction with an in-phase 30 Hz 1.0 mm sinusoidal vibration in the x direction. Supposing our goal is to end up with a part lying with its long face on the table, this vibration seems to work. The simulation data suggest that the vibration successfully destabilizes the 0° orientation without destabilizing the 90° orientation. After 0.8 s of simulated vibration, some parts remain upright while their neighbors have fallen. After 3.0 s of simulated time, all initial conditions are attracted to the desired 90° orientation. A closer look at the data from which the pictures in Figure 2 are taken suggests that there are rather complicated transients. The vibrations appear to cause an intermittent resonance in the parts with orientations near 0° whose magnitude increases until the orientation is destabilized.

Table I illustrates the results of several such simulations. Noting that the relative impact velocity increases proportionately both with vibration frequency and amplitude, one might expect these parameters to give rise to similar behavior. However, these simulations instead demonstrated that such an easy generalization cannot be confirmed. The simulation labeled "chaotic" was capable of reorienting parts back and forth between the 0° and 90° stable states.

Analysis of why some vibrations are more effective than others is difficult for the following reasons. The impact model [32] has 5 dynamically distinct contact modes whose selection depends not only on the system parameters but also on the state of the system at impact. Due to the quadratic form of Newtonian flight and the sinusoidal form of the part rotation and table vibration, the flight time between impacts cannot be expressed in closed form. The varying time between impacts makes a standard sampled-data approach impossible. Thus while analysis is clearly possible, it will not be straightforward. Yet, these simulations demonstrate that, even for such a simply shaped part, finding an effective vibration strategy is by no means straightforward. The success of this simulation encourages further study of the problem, and the apparent sensitivity of the vibration strategy demands it. We are now motivated to investigate a still simpler setting of the problem.

2.1.2. The one-degree-of-freedom simplification. The one-degree-of-freedom problem shown in Figure 4 removes all orientation: the part and table are both constrained to move

Table I Sensitivity to Horizontal and Vertical Sinusoidal Vibrations

x Frequency, Magnitude	*All Parts Lying Down*
15 Hz 2 mm	4.0 s
15 Hz 4 mm	"chaotic"
30 Hz 1 mm	2.9 s
30 Hz 2 mm	2.1 s
60 Hz 0.1 mm	5.0 s
60 Hz 1 mm	3.1 s

Note: Times indicate approximate onset of steady state where all initial orientations have evolved to the 90° orientation. "Chaotic" denotes a vibration in which both statically stable orientations were destabilized and no simple steady-state behavior emerged. The y vibrations used were 60 Hz 0.2 mm.

in the y direction, and the goal is to choose a table motion which brings the part into a specified periodic vertical trajectory. The hope here is that the nature of vertical table trajectories that bring a point mass to a specified repeated height at apex will have some relationship to vertical and horizontal trajectories that bring a rigid mass to a specified orientation. Our simulations suggest that, by careful parameter selections, we can create globally attracting trajectories even for three-degree-of-freedom systems. We hope analytically to prove global results in these systems as well.

Here we seek to demonstrate global stability of a desired bouncing state for a particular one-degree-of-freedom juggling scheme. It should be noted that, although this problem is far simpler than that of the previous three-degree-of-freedom setting, it has spawned a large and growing analytical literature [14,16,19,28,29,34].

Sinusoidal motions [28] have an extensive background in this literature, but study of their dynamics has been mostly limited to system parameters leading to chaotic motion. Local stability of the Shannon juggler [24] has been established: we seek a global result motivated by the intended application. To our knowledge, ours represents the first effort in the literature to obtain a globally asymptotically stable period one orbit.

2.2. The One-Degree-of-Freedom Problem

Figure 3 shows the results of a one-degree-of-freedom simulation of the evolution of the boundary of the attracting energy region, R, described later, in section 4. This simulation provided the basic understanding of the system which led to the analysis in the sequel.

We will first describe the setup in words alongside the formal notation that appears in the analysis below. We will next introduce the physical models that underlie this analysis.

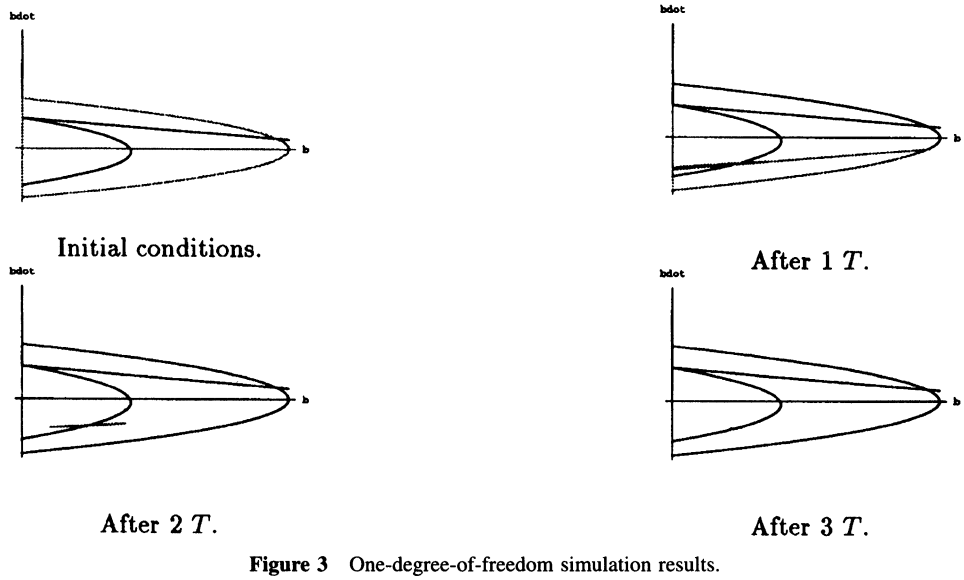

Figure 3 One-degree-of-freedom simulation results.

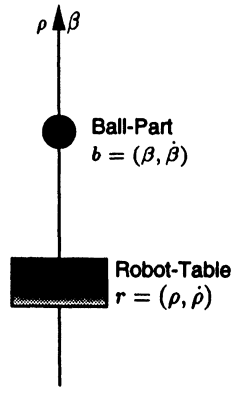

Figure 4 Setup for the one-degree-of-freedom ball-part orientation problem.

Appendix section B.7 lists the notation we employ to represent the one-degree-of-freedom version of the problem depicted in Figure 4.

For the remainder of the discussion, the terms "robot" and "table" (henceforth "robot-table") will be treated as synonymous, as are the terms "ball" and "part" (henceforth "ball-part").

2.2.1. Notational preview. $\mathcal{H}$ denotes the region $\overline{\beta} > 0$ on the $(\overline{\beta}, \dot{\overline{\beta}})$ plane, the physically realistic part of the state space in which the ball-part is on or above the robot-table. The part of the state space not in $\mathcal{H}$ is not physically realizable and will be ignored in the remainder of this paper. $\mathcal{H}$ is shown in Figure 5.

We will introduce an impact model and use the $\mathcal{H}$ half-plane to plot the iterates of successive impact states. Looking ahead, $\mathcal{B}_1$ denotes the region in $\mathcal{H}$ (defined by $0 \leq \tau_c(b) < T$) within which the ball-part will strike the robot-table within one period. $\mathcal{B}_2$ is defined as the $\mathcal{H}$–$\mathcal{B}_1$ region ($T \leq \tau_c$), in which the ball-part will not strike the robot-table within one period. The boundary line, $\partial\mathcal{B}_2$, between $\mathcal{B}_1$ and $\mathcal{B}_2$ (defined by $\tau_c = T$) is by

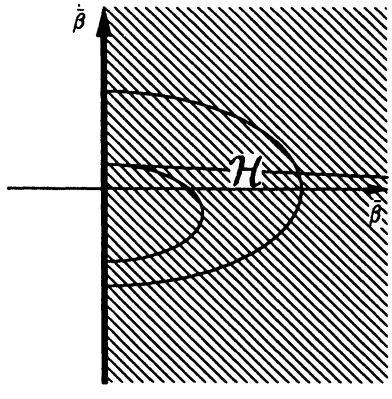

Figure 5 $\mathcal{H}$ regions.

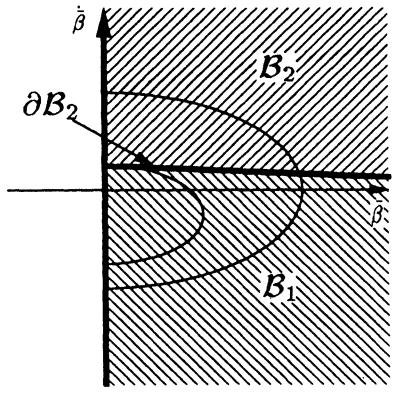

Figure 6 $\mathcal{B}_1$ and $\mathcal{B}_2$ regions.

definition contained within $\mathcal{B}_2$. The part of the $\dot{\bar{\beta}} = 0$ axis below the $\partial\mathcal{B}_2$ line is explicitly contained within $\mathcal{B}_1$, while the part of the axis above the $\partial\mathcal{B}_2$ line is contained in $\mathcal{B}_2$. These regions are depicted in Figure 6.

Figure 7 indicates the level curves of the ball-part's total energy function, $E(\bar{b})$, defined in section 3.4. During free flight, the ball-part state moves along these lines in the direction shown by the arrows.

In $\mathcal{B}_1$, E is changed at impact, except on a parabolic curve which we denote as

$$\mathcal{B}_1^0 := \{\bar{b} \in \mathcal{B}_1 \mid \Delta E(\bar{b}) = 0\}$$

as depicted in Figure 8. In the same figure, a new region $\mathcal{R}$ is shown, which will figure prominently in the sequel. In particular, these curves are important for the global attraction analysis presented later.

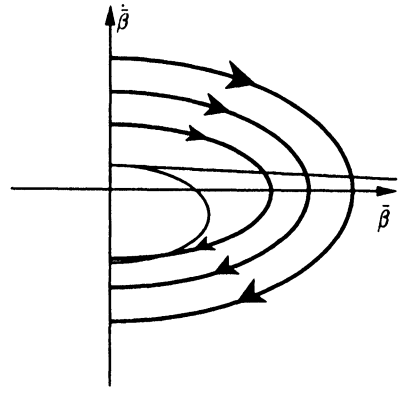

Figure 7 Constant energy lines/free flight trajectories.

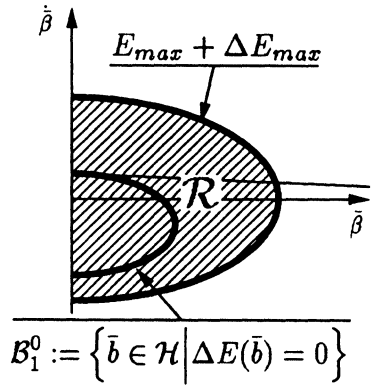

Figure 8 Important energy related lines.

2.2.2. Physical models. The state of an arbitrary one-degree-of-freedom mass is denoted $x = (\chi, \dot{\chi}) \in \mathbf{R}^2$. Newton's equation of free flight,

$$\ddot{x} = -\gamma,$$

gives, upon two integrations, a map on the plane,

$$\begin{aligned} F^t(x) &= A_t x - a_t \\ A_t &:= \begin{bmatrix} 1 & t \\ 0 & 1 \end{bmatrix} \\ a_t &:= \gamma t \begin{bmatrix} t/2 \\ 1 \end{bmatrix}, \end{aligned} \tag{1}$$

indexed by the time of flight t, which we shall use throughout the discussion.

For the purpose of analysis, we assume that impacts occur on a very short time scale compared to the system dynamics, so that velocity changes at impact are effectively instantaneous. Suppose the point mass x loses some energy (through deformation, sound, etc.) during an impact with another point mass y in a manner captured by the *coefficient of restitution* (α),

$$\begin{aligned} \dot{\chi}' &= \alpha \dot{\chi} \\ 0 < \alpha &< 1 \\ \chi &= x - y \end{aligned} \tag{2}$$

where $\dot{\chi}$ and $\dot{\chi}'$ are the relative point mass velocities of the masses immediately before and immediately after impact, respectively.

If x collides with a much more massive body, y, then the massive body's state is unchanged by the impact whereas, the new state of smaller body is given by

$$C_y(x) = R_\alpha x + (I - R_\alpha) y$$

$$R_\alpha := \begin{bmatrix} 1 & 0 \\ 0 & -\alpha \end{bmatrix}. \tag{3}$$

2.3. The Effective Environmental Control System

The system shown in Figure 4 consists of a one-degree-of-freedom "robot-table,"

$$r = (\rho, \dot{\rho})$$

and a lighter "ball-part,"

$$b = (\beta, \dot{\beta})$$

falling in the earth's gravitational field and constrained to move in the direction of gravitational field gradient (vertically). The ball-part falls from some initial position and velocity, b, according to Newton's law (1) and reacts to a collision with the robot-table at some state r according to the coefficient of restitution law (3).

Now let b denote the state of the ball-part just prior to an impact. Suppose the robot-table impacts with velocity u_2 and allows the ball-part to fall freely for the next u_1 interval of time. Then the state of the ball-part just prior to the next impact is given by

$$f(b, u) := F^{u_1} \circ C_{u_2}(b) \tag{4}$$

Any effect of the robot-table on the ball-part may be described with regard to this model, which is, in effect, a discrete dynamical control system. In this paper, we find it more convenient to sample the ball-part's trajectory at state $\bar{b}$, when the robot-table is at the minimum ρ of it's motion, as shown in Figure 9.

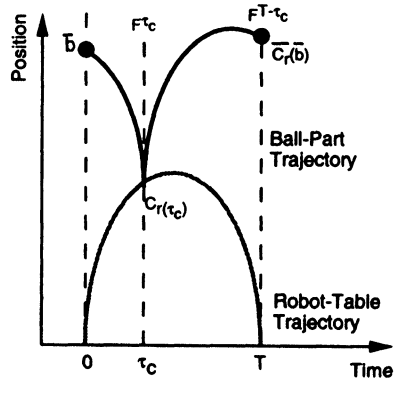

Figure 9 Coupled oscillators.

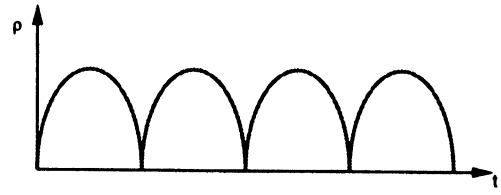

Figure 10 A lossless relaxation oscillator.

3. LOCAL ANALYSIS OF A SIMPLE JUGGLER

A parabolic robot-table trajectory was chosen primarily for ease of analysis: the time to collision, τ_c, is a closed-form expression, which simplifies the remainder of the analysis. Unfortunately, this type of trajectory is not physically realizable due to the discontinuous jumps in velocity, which also results in a discontinuity in the iteration function. In the future we hope to use a similar strategy to prove global stability for a more realistic sinusoidal robot trajectory, for which the time of collision expression cannot be exhibited in closed form [28].

3.1. The Robot-table's Strategy: A Lossless Relaxation Oscillator

Consider a robot-table control strategy that induces the relaxation oscillator depicted in Figure 10, independent of the ball-part's state. This trajectory characterizes the behavior of a perfectly elastic point mass, $r(t) = (\rho, \dot{\rho})(t)$, bouncing in the earth's gravitational field subject to lossless collisions with the ground at impact and lossless free flight in between. Fixing coordinates, say the robot-table collides with the ground at time $t = 0$, in the state $-r_0 = (0, -\dot{\rho}_0)$. Lossless collisions correspond to coefficient of restitution unity, so that the evolution of the robot-table's state from zero height at the "post bounce" velocity, $\dot{\rho}_0$, is now given by

$$r(t) = F^{\tau_p(t)}(r_o) \tag{5}$$

where τ_p denotes time modulo the period of flight,[3] $T := 2\dot{\rho}_0/\gamma$. The parameter ρ_0 is assumed positive throughout the sequel.

[3] That is, τ_p denotes the piecewise linear periodic function coincident with the identity on the interval $0 \leq t < T$.

3.2. Coupling the Ball-part: A Lossy Relaxation Oscillator

Suppose now that a much lighter point mass is constrained to fall along the same vertical axis as the previous one. Denote its position and velocity by $\bar{b} = (\bar{\beta}, \dot{\bar{\beta}})$, measured at the moment the heavy point mass just touches the ground, $\tau_p = 0$.[4] Again, we will suppose no energy losses in flight.[5]

There is a region, $\mathcal{B}_1 \subset \mathcal{H}$, in the ball-part's state space, such that if $\bar{b} \in \mathcal{B}_1$ then there will be a collision with the robot-table,[6]

$$\begin{aligned} 0 &= [F^{\tau_c}(\bar{b})]_1 - [F^{\tau_c}(r_0)]_1 \\ &= [A_{\tau_c}(\bar{b} - r_0)]_1 \\ &= \bar{\beta} + \tau_c(\dot{\bar{\beta}} - \dot{\rho}_0) \end{aligned}$$

before the robot-table next touches the ground. Solving this equation for τ_c gives the function,

$$\tau_c(\bar{\beta}, \dot{\bar{\beta}}) := \frac{\bar{\beta}}{\dot{\rho}_0 - \dot{\bar{\beta}}}, \tag{6}$$

that computes the time to collision. Imposing the inequalities

$$0 \leq \tau_c(\bar{b}) \leq T,$$

makes explicit the extent of the region $\mathcal{B}_1$,

$$\mathcal{B}_1 := \{\bar{b} \in \mathcal{H} \mid [\tfrac{1}{2}\gamma, \dot{\rho}_0] \begin{bmatrix} \bar{\beta} \\ \dot{\bar{\beta}} \end{bmatrix} < \dot{\rho}_0^2\} \tag{7}$$

The state of such a ball-part at the time, T, of the robot-table's next collision with ground (at state $-r_0$), may now be modeled by flying the two masses to collision, $C_F \tau c_{(r_0)} \circ F^{\tau_c}(\bar{b})$, and then flying the ball-part onward for time $T - \tau_c$. This yields a map $F^T \circ \bar{C}_{r_0}(\bar{b})$ where

$$\bar{C}_r(\bar{b}) := F^{-\tau_c(\bar{b})} \circ C_{F^{\tau_c}(\bar{b})(r)} \circ F^{\tau_c(\bar{b})}(\bar{b}) \tag{8}$$

---

[4] Note that the barred variables $\bar{b}$, $\bar{\beta}$, $\dot{\bar{\beta}}$ are simply samples of the unbarred variables b, β, $\dot{\beta}$ introduced in section 2.3.

[5] This is shown later in section 3.4.

[6] Denoted in the following by equating the position components—$[\cdot]_1$—of both balls.

Note that

$$\overline{C}_r(\overline{b}) = A_{[-\tau_c]} R A_{\tau_c}(\overline{b} - r_0) + r_0.$$

By definition of τ_c, it follows that both

$$A_{\tau_c}(\overline{b} - r_0) = \begin{bmatrix} 0 \\ \dot{\overline{\beta}} - \dot{\rho}_0 \end{bmatrix},$$

and

$$\alpha\overline{\beta} = -\alpha\tau_c(\dot{\overline{\beta}} - \dot{\rho}_0),$$

so that

$$\overline{C}_{r_0}(\overline{b}) = -\alpha(\overline{b} - r_0) + r_0 \tag{9}$$

and

$$F^T \circ \overline{C}_{r_0}(\overline{b}) = -\alpha A_T(\overline{b} - r_0) - r_0.$$

3.3. Local Stability Analysis of the Coupled Oscillator System

If the next state of the ball-part after the first collision is also in β_1 then its state after a second collision is given by composing the last function with itself. Assuming that all further iterates, remain in β_1 as well, it would follow that the state of the ball-part at the time of the robot-table's k^{th} bounce with the ground is given by the recursion

$$\begin{aligned} \overline{b}_{k+1} &= \overline{f}_1(\overline{b}_k) \\ &:= -\alpha A_T \overline{b}_k + (\alpha - 1) A_{-\xi 1} r_0 \end{aligned} \tag{10}$$

where $\xi_1 := \alpha T/(1 - \alpha)$. We now demonstrate the existence of an open set of points in β_1 whose iterates remain in that set.

The map, $\overline{f}_1$, has a unique fixed point,

$$\begin{aligned} e_1 &:= -(I + \alpha A_T)^{-1} \cdot (1 - \alpha) A_{-\xi 1} r_0 \\ &= -\frac{1 - \alpha}{1 + \alpha} A_{-\epsilon 1} r_0 \end{aligned}$$

where $\epsilon_1 := 2\alpha T/(1 - \alpha^2)$. Now

$$e_1 = \begin{bmatrix} \dfrac{4\alpha\dot{\rho}_0^2}{(1+\alpha)^2\gamma} \\ \dfrac{-(1-\alpha)\dot{\rho}_0}{1+\alpha} \end{bmatrix} \in \beta_1,$$

since the first component is positive (i.e., $e_1 \in \mathcal{H}$) and

$$\tau_c(e_1) < T.$$

Moreover, $-\alpha A_T$ has eigenvalues inside the unit circle for any choice of $\dot{\rho}_0$. Thus, some open neighborhood of e_1 remains in $\mathcal{B}_1$ under iteration by $\bar{f}_1$. This open neighborhood takes e_1 as its limit.

3.3.1. Extending $\bar{f}$ to $\mathcal{H}$. There is a second region, $\mathcal{B}_2 = \mathcal{H} - \mathcal{B}_1$, in the ball-part's state space such that

$$T \leq \tau_c(\bar{b})$$

and

$$\mathcal{B}_2 := \{\bar{b} \in \mathcal{H} \mid T \leq \tau_c(\bar{b})\} \tag{11}$$

and no impact occurs in the next table oscillation period. When this condition holds, we may define

$$\bar{f}_2 := F^T \tag{12}$$

We may then define a global discrete-time function $\bar{f}$ on $\mathcal{H}$:

$$\bar{f} := \begin{cases} \bar{f}_1 & :\bar{b} \in \mathcal{B}_1 \\ \bar{f}_2 & :\bar{b} \in \mathcal{B}_2 \end{cases} \tag{13}$$

Note (unfortunately) that $\bar{f}$ is not continuous—a consequence of the velocity discontinuity of the robot-table's trajectory in Figure 9.

3.4. Total Energy and Energy Change

Presented here are elementary results regarding energy within the system which are critical to the global stability analysis.

3.4.1. Total energy. We make use of the fact that total energy is preserved whenever flight dynamics are applicable. (We ignore any dissipative effects in flight).

Defining:

$$E(\bar{b}) := \gamma\bar{\beta} + \frac{1}{2}\dot{\bar{\beta}}^2, \tag{14}$$

and

$$E_0 := E(\bar{b}_0)$$

$$= \gamma\bar{\beta}_0 + \frac{1}{2}\dot{\bar{\beta}}_0^2,$$

flight dynamics imply

$$\bar{b}(t) = F^t \circ \bar{b}_0,$$

and we have

$$E(t) := E \circ F^t$$

$$= \gamma(\bar{\beta}_0 + \dot{\bar{\beta}}_0 t - \frac{1}{2}\gamma t^2)$$

$$+\frac{1}{2}(\dot{\bar{\beta}}_0 - \gamma t)^2,$$

which reduces to

$$E(t) = \gamma\bar{\beta}_0 + \frac{1}{2}\dot{\bar{\beta}}_0^2$$

$$= E_0 .$$

Therefore, under $\bar{f}$ energy is conserved in the region $\mathcal{B}_2$

$$E \circ \bar{f}\,|_{\mathcal{B}_2} = E \tag{15}$$

3.4.2. Energy change. We define an energy change function ΔE,

$$\Delta E(\bar{b}) := E \circ \bar{f}(\bar{b}) - E(\bar{b})$$

$$= \begin{cases} \Delta_1 E := \Delta E\,|_{\mathcal{B}_1} & : \bar{b} \in \mathcal{B}_1 \\ \Delta_2 E := \Delta E\,|_{\mathcal{B}_2} & : \bar{b} \in \mathcal{B}_2 \end{cases}$$

which expresses the energy change caused by $\bar{f}$. From (15), we know that $\Delta_2 E \equiv 0$. Thus we need only be concerned with $\Delta_1 E$.

Referring back to (8), since energy is conserved during free flight and potential energy is conserved during impact, all energy changes must take place in the kinetic energy at impact. According to (1) and (3), the energy change may be expressed as:

$$\Delta_1 E = \frac{1}{2}[-\alpha\dot{\bar{\beta}} + \alpha\gamma\tau_c$$

$$+(1+\alpha)\dot{\rho}_0 - (1+\alpha)\gamma\tau_c]^2 \qquad (16)$$

$$-\frac{1}{2}(\dot{\bar{\beta}} - \gamma\tau_c)^2$$

3.5. Fixed Points

The existence of the e_1 fixed point in $\bar{f}_1$ was shown in section 3.3. However, there may be a large number of fixed points of $\bar{f}$ which we consider in this section.

3.5.1. Existence of fixed points. Aside from the period T fixed point e_1, there are fixed points, e_K, of period KT for the composite map $\bar{f}_1 \circ \bar{f}_2^{K-1}$. We call these fixed points "subharmonic" because they represent trajectories which impact the robot-table only once every K time periods.[7]

These subharmonic fixed points must satisfy two conditions. The first requires that time of flight, $t_f = 2\beta/\gamma$, must be an integer multiple of the robot-table period, T, so that $t_f = KT$:

$$\dot{\beta} = \frac{1}{2}K\gamma T$$

The second requires that velocity be conserved in the restitution balance equation (33), resulting in:

$$\dot{\rho}(\tau_c) = \frac{1}{2}\,\frac{1-\alpha}{1+\alpha}K\gamma T \qquad (17)$$

$$= \frac{1-\alpha}{1+\alpha}K\dot{\rho}_0$$

Whenever the robot-table velocity at impact, $\dot{p}(\tau_c)$, is high enough to satisfy (17) for a given K, there exists a period K fixed point, e_K. Since the maximum robot-table velocity is limited, we can define the maximum fixed point period, K_{max} :

$$K_{max} := \left\lfloor \max_{\dot{\rho} \le \dot{\rho}_0} \left| \frac{1+\alpha}{1-\alpha}\,\frac{\dot{\rho}}{\dot{\rho}_0} \right| \right\rfloor \qquad (18)$$

$$= \left\lfloor \frac{1+\alpha}{1-\alpha} \right\rfloor$$

[7] Note that "harmonic" fixed points, in which the ball-part impacts the robot-table multiple times in a oscillation period, are not possible under our formulation. Because the ball-part and the robot-table operate under the same gravitational field, $\dot{\beta} > \dot{\rho}$ after the first impact and it is impossible for a second impact to occur before the end of the period.

3.5.2. Maximum energy of fixed points. In order to allow fixed points up to period K, (18) requires that

$$K \leq K_{max} < K + 1 \tag{19}$$

When the definition of K_{max}, (18), is inserted into (19), the resulting condition which restricts the set of fixed points to $\{e_k | k \leq K\}$ is:

$$\frac{K-1}{K+1} \leq \alpha < \frac{K}{K+2} \tag{20}$$

To limit our attention to only a period 1 fixed point, (20) shows[8]

$$0 < \alpha < \frac{1}{3} \tag{21}$$

A question to consider at this point is whether this range of α is reasonable. We believe it is possible to decrease the restitution coefficient by using an energy-absorbent covering on the robot-table. It is easy to reduce the restitution coefficient in this manner without changing the material properties of the ball-part.

3.5.3. Local stability of fixed points. As noted in section 3.5.1, period K fixed points exist on the composite map $\bar{f}_1 \circ \bar{f}_2^{K-1}$. It is readily determined that the Jacobian of the composite map is

$$-\alpha A_T^K = \begin{bmatrix} -\alpha & -\alpha T^K \\ 0 & -\alpha \end{bmatrix}$$

and the eigenvalues are within the unit circle for all physical α. Thus, every fixed point that meets the existence criteria in section 3.5.1 is locally stable.

4. GLOBAL STABILITY ANALYSIS

This section contains a demonstration of the global stability of the e_1 fixed point, assuming favorable parameter values.

4.1. Attracting Energy Boundary

As discussed in section 3.4, every point in the β_1 region experiences an energy change caused by impact during the next table period. A zero-energy-change boundary β_1^0 can be

[8] Note that the possibility of $\alpha = 0$ is not applicable to the problem considered.

defined by $\Delta_1 E = 0$ from (16) as

$$\mathcal{B}_1^0 := \left\{ \bar{b} \in \mathcal{H} \;\middle|\; \dot{\bar{\beta}} = \gamma\tau_c - \frac{1+\alpha}{1-\alpha}(\dot{\rho}_0 - \gamma\tau_c) \right\} \tag{22}$$

This zero-energy-change boundary partitions $\mathcal{B}_1$ into three regions, as shown in Figure 11: a region $\mathcal{B}_1^+$ which gains energy after impact ($\Delta_1 E > 0$), a region $\mathcal{B}_1^-$ which sheds energy after impact ($\Delta_1 E < 0$), and $\mathcal{B}_1^0$.

We use the maximum E on the $\mathcal{B}_1^+ \cup \mathcal{B}_1^0$ region, defined in equation (34) from Appendix section A.1,

$$E_{max} = \frac{1}{2}\left(\frac{1+\alpha}{1-\alpha}\dot{\rho}_0\right)^2$$

This value represents the maximum ball-part energy that the robot-table can maintain. We also use the maximum ΔE on the $\mathcal{B}_1^+ \cup \mathcal{B}_1^0$ region, defined in equation (37) from Appendix section A.2,

$$\Delta E_{max} = \frac{1}{2}\,\frac{1+\alpha}{1-\alpha}\,\dot{\rho}_0^2$$

This value represents the maximum ΔE on $\mathcal{H}$. Combining these values results in

$$E_{max} + \Delta E_{max} = \frac{1+\alpha}{(1-\alpha)^2}\,\dot{\rho}_0^2.$$

A conservative estimate of the attracting energy region $\mathcal{R}$ can then be obtained with respect to the function

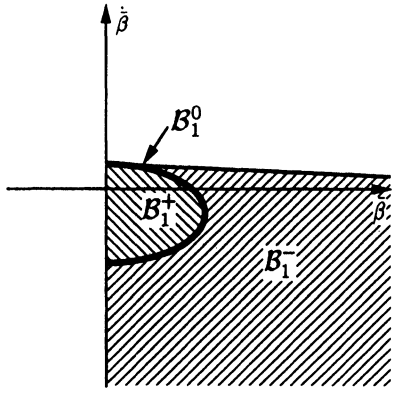

Figure 11 Impact energy regions in $\mathcal{B}_1$

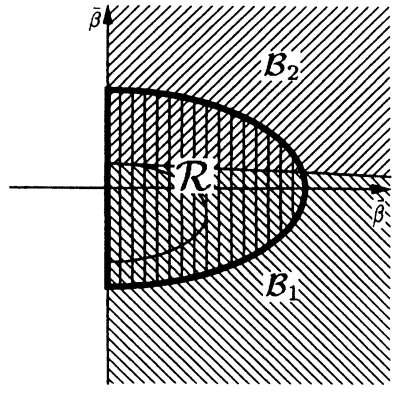

Figure 12 The regions $\mathcal{R}$, $\mathcal{B}_1$, and $\mathcal{B}_2$.

$$R(\bar{b}) := E_{max} + \Delta E_{max} - E(\bar{b}) \tag{23}$$

$$= \frac{1+\alpha}{(1-\alpha)^2}\dot{\rho}_0^2 - \gamma\bar{\beta} - \frac{1}{2}\dot{\bar{\beta}}^2.$$

$$R := \left\{\bar{b} \in \mathcal{H} \,\middle|\, R(\bar{b}) \geq 0\right\} \tag{24}$$

where $E(\bar{b})$ is as defined in (14).

Proposition 1. If (21) holds, then $\mathcal{R}$ (24) is a globally attracting invariant set.

Proof. By construction, all points in the region $\mathcal{B}_1 - \mathcal{R}$ also lie in the region $\mathcal{B}_1^-$ (See Figures 11, 12). According to (1), all points in $\mathcal{B}_2$, and hence in $\mathcal{B}_2 - \mathcal{R}$, move along invariant energy trajectories (free flight) to the region $\mathcal{B}_1 - \mathcal{R}$. Therefore, all points external to $\mathcal{R}$ are attracted to $\mathcal{R}$ as they lose energy at successive impacts. In fact, all finite states are drawn into the $\mathcal{R}$ region in finite time.

Pick any finite state $\bar{b}_0 \in \mathcal{H} - \mathcal{R}$. Remembering the definition of energy in (14), we then define the energy of $\bar{b}_0$ as $E(\bar{b}_0)$. We then define the worst-case time to impact, τ_w:[9]

$$\tau_w := \frac{2}{\gamma}\sqrt{2E(\bar{b}_0)}. \tag{25}$$

Referring to Appendix section A.4, the worst-case number of impacts before $\bar{b}_0$ enters $\mathcal{R}$ is given by $\left\lceil \frac{E(\bar{b}_0) - E_{max} - \Delta E_{max}}{-\Delta E_{sup}} \right\rceil$. Noting that states with less energy also have shorter times between impacts, the maximum time between impacts is given by τ_w, from (25). Thus the maximum time it will take for any given finite initial state in $\mathcal{H} - \mathcal{R}$ to enter

[9] Note that $\tau_w = \tau_c(\bar{b}_0)$ if $\bar{\beta}_0 = 0$ and $\bar{b}_0$ is in the $\mathcal{B}_2$ region, and τ_w is an integer multiple of T. Otherwise, $\tau_w > \tau_c(\bar{b}_0)$.

$\mathcal{R}$ is given by:

$$t_R := \frac{2}{\gamma}\sqrt{2E(\bar{b}_0)}\left\lceil \frac{E(\bar{b}_0) - E_{max} - \Delta E_{max}}{-\Delta E_{sup}} \right\rceil. \tag{26}$$

Because of the worst-case assumptions of flight time and $\Delta_1 E$, states are typically attracted to $\mathcal{R}$ in a much shorter time than t_R.

Once a trajectory is trapped within the $\mathcal{R}$ region it cannot leave. The highest energy possible within the $\mathcal{B}_1^+ \cup \mathcal{B}_1^0$ region is E_{max}. The highest energy gain possible within the $\mathcal{B}_1^+$ region is ΔE_{max}. Adding $E_{max} + \Delta E_{max}$ does not provide sufficient energy to leave $\mathcal{R}$. Therefore, $\mathcal{R}$ is attracting and invariant under $\bar{f}$.

4.3. Global Attraction to $\mathcal{K} \subset \mathcal{R}$

In this section, we show that all trajectories rapidly decay to another invariant set, $\mathcal{K}$, after they enter $\mathcal{R}$.

4.3.1. Relative kinetic energy decreases in $\mathcal{R}$. Once a trajectory has entered $\mathcal{R}$, it can be shown that the trajectory rapidly approaches a constant kinetic energy (constant $\dot{\bar{\beta}}$) at each impact, as shown in Figure 3. In order to prove this, it is useful to perform a change of coordinates:

$$z = b - e_1 \tag{27}$$

where e_1 is the period 1 fixed point of the return map. The z_k series follows the same linear dynamics as the b_k series for points in the $\mathcal{R} \cap \mathcal{B}_1$ region:

$$\begin{aligned} z_{k+1} &= b_{k+1} - e_1 \\ &= -\alpha A_T b_k + (\alpha - 1)A_{-\xi} r_0 - e_1 \\ &= -\alpha A_T b_k + \alpha A_T e_1 \\ &= -\alpha A_T z_k \end{aligned}$$

Noting that kinetic energy[10], K, may be expressed

$$K(z) = \frac{1}{2}(u_2' z)^2 \tag{28}$$

[10] Note that this definition of the kinetic energy K is distinct from the integer K used in the fixed-point discussion of section 3.5.

it is possible to write

$$\Delta K = K \circ f - K$$

and

$$\begin{aligned}
\Delta K(z_z) &= K \circ f(z_k - K(z_k) \\
&= K(-\alpha A_T z_k) - K(z_k) \\
&= \frac{1}{2}(-\alpha u_2' A_T z_k)^2 - \frac{1}{2}(u_2' z_k)^2 \\
&= \frac{1}{2}((-\alpha u_2' z_k)^2 - (u_2' z_k)^2) \\
&= \frac{1}{2}(\alpha^2 - 1)(u_2' z_k)^2
\end{aligned}$$

so that for $0 \leq \alpha < 1$,

$$\Delta K < 0$$

Since $K \geq 0$ and $\Delta K < 0$, LaSalle's theorem states that

$$\lim_{k \to \infty} K(z_k) = 0$$

Furthermore, the change of coordinates defined in (27) requires that

$$\lim_{k \to \infty} K(b_k) = K(e_1).$$

Since $\bar{f}_2$ applies on $\mathcal{R} \cap \mathcal{B}_2$, trajectories in this region also approach $K(e_1)$ during free flight (Fig. 7).

In plain English: the kinetic energy of an orbit within the $\mathcal{R}$ region rapidly approaches the kinetic energy of the $\mathcal{B}_1$ fixed point, e_1.

4.3.2. The attracting invariant set $\mathcal{K}$. Now parameterize the $\partial\mathcal{B}_2$ line as

$$\dot{\bar{\beta}} = \begin{bmatrix} 1 & \\ & -\frac{1}{T} \end{bmatrix} \bar{\beta} + \dot{\rho}_0 \tag{29}$$

The intersection of $\partial\mathcal{B}_2$ with the line defined by the kinetic energy of the fixed point, e_1, occurs at the point p:

$$p := \begin{bmatrix} \frac{2T}{1+\alpha}\dot{\rho}_0 \\ -\frac{1-\alpha}{1+\alpha}\dot{\rho}_0 \end{bmatrix}, \tag{30}$$

as shown in Figure 13. Since

$$\begin{aligned} E(p) &= \frac{2T}{1+\alpha}\dot{\rho}_0\gamma + \frac{1}{2}\left(-\frac{1-\alpha}{1+\alpha}\dot{\rho}_0\right)^2 \\ &> E_{max} + \Delta E_{max}, \end{aligned} \tag{31}$$

we note that $p \notin \mathcal{R}$. Thus, points with kinetic energy near the fixed point within the $\mathcal{R}$ region are in the $\mathcal{B}_1$ region, and the dynamics of $\bar{f}_1$ apply.

We define a region $\mathcal{K}$, within the $\mathcal{R}$ region with kinetic energy close to the fixed point (Figure 14),

$$\mathcal{K} := \left\{ \bar{b} \in B_1 \,\middle|\, K\left(\bar{b} - e_1\right) \leq \epsilon \right\} \cap R, \tag{32}$$

where $K(\bar{b})$ is as defined in (28). Now note that $\bar{f}_1(\partial\mathcal{K}) \subset \mathcal{K}$, since K is decreasing (section 4.3.1) and $\bar{f}_1(\partial\mathcal{R} \cap \mathcal{B}_1) \subset \mathcal{R}$ (section 4.2). Since $\bar{f}|_{\mathcal{K}} = \bar{f}_1$ is continuous, we now conclude that $\bar{f}(\mathcal{K}) \subseteq \mathcal{K}$. Moreover, $\mathcal{K}$ attracts all of $\mathcal{R}$ under $\bar{f}$ since K is decreasing on $\mathcal{R}$.

4.4. Fixed Point Is a Global Attractor

Since $\bar{f}|_{\mathcal{K}} = \bar{f}_1$ is linear, the stable fixed point, e_1, attracts all of $\mathcal{K}$. Since $\mathcal{K}$ is a globally attracting invariant set, we conclude that e_1 attracts all of $\mathcal{H}$.

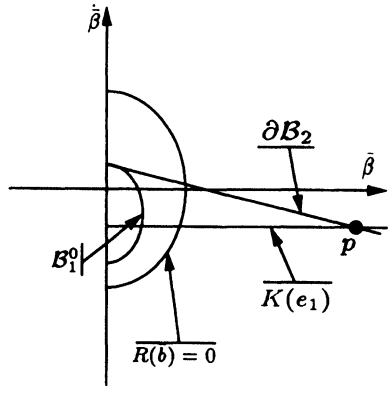

Figure 13 Some important curves and their intersections.

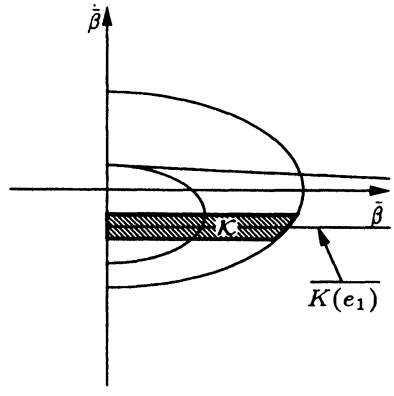

Figure 14 The region.

5. CONCLUSION

We have found a parameter range for the coefficient of restitution that insures the global asymptotic stability of a specified period one orbit—a bouncing motion—of a ball subject to excitations from an oscillating table. In contrast, this physical setup has traditionally been studied as providing a classic example of chaotic dynamics. Our positive result encourages further investigation of this approach to the parts-feeding problem.

In the problem studied here, the table is assumed to behave as a perfectly elastic (lossless) bouncing ball. This is not a motion that an industrial machine can reliably reproduce, and our next analytical efforts will be directed at finding a more realistic sinusoidal motion resulting in global stability. Should our three-degree-of-freedom experiments corroborate the suggestive simulation results described here, we will seek to generalize this analysis to the three-degree-of-freedom and six-degree-of-freedom problems.

Acknowledgements

We wish to thank Deneb Robotics for their assistance in the form of their Igrip robotic simulation software used for the three-degree-of-freedom table simulation.

References

1. R. L. Andersson. Understanding and applying a robot ping-pong player's expert controller. In *Proceedings 1989 International Conference on Robotics and Automation*, Scottsdale, AZ, 1989, pp. 1284–1289.
2. *Assembly Automation: Proceedings of the 8th International Conference*, Springer Verlag, New York, March, 1988.
3. Böhringer, K. F. V. Bhatt, and K. Goldberg. *Sensorless manipulation using transverse vibrations of a plate.* (Submitted to ICRA 95), May 1995.
4. Boothroyd, G. *Assembly automation and product design.* Marcel Dekker, New York, 1992.

5. Boothroyd, G. C. Poli, and L. E. Murch. *Automatic assembly*. Marcel Dekker, New York, 1982.
6. Brost, R. *A Cad-based approach to general-purpose part feeders*. Presented at the Robotic Industries Association Flexible Parts Feeding Workshop, October, 1993.
7. Bühler, M. D. Koditschek, and P. Kindlmann. A family of robot control strategies for intermittent dynamical environments. *IEEE Control Systems Magazine*, ***10(2)*** (February, 1990).
8. Canny, J. and K. Goldberg. "RISC" for industrial robotics: Recent results and open problems. In *IEEE International Conference on Robotics and Automation*, May, 1994.
9. Daum, R. *Machine vision lighting for flexible parts feeding*. Presented at the Robotic Industries Association Flexible Parts Feeding Workshop, San Jose, CA, October 1993.
10. den Hamer, H. E. *Interordering: A new method of component orientation*, vol. 2 of *Studies in mechanical engineering*. Elsevier Scientific Publishing, New York, 1980.
11. Erdmann, M. and M. T. Mason. An exploration of sensorless manipulation. In *Proc. IEEE International Conference on Robotics and Automation*, San Francisco, April, 1986, pp. 1569–1574.
12. Farnum, G. *Delivering the part*. Presented at the Robotic Industries Association Flexible Parts Feeding Workshop, October, 1993. (Quote attributed to Bill Davis, President of Feeder Systems).
13. Grossman, D. and M. Blasgen. Orienting mechanical parts by computer-controlled manipulator. *IEEE Transactions on Systems, Man, and Cybernetics*, September, 1975, pp. 561–565.
14. Guckenheimer, J. and P. Holmes. *Nonlinear oscillations, dynamical systems, and bifurcations of vector fields*, vol. 42 of *Applied mathematical sciences*. Springer-Verlag, New York, 1983.
15. Koditschek, D. and M. Bühler. Analysis of a simplified hopping robot. *International Journal of Robotics Research*, ***10(6)*** (December, 1991).
16. Kowalik, Z. M. Franaszek, and Pi. Pierański. Self-reanimating chaos in the bouncing-ball system. *Physical Review A*, ***37(10)*** (May 1988), *4016–4022.*
17. McGeer, T. *Passive bipedal running*. Technical Report IS-TR-89-02, Simon Fraser University, Centre for Systems Science, April, 1989.
18. Natarajan, B. K. Some paradigms for the automated design of parts feeders. *International Journal of Robotics Research*, ***8(6)*** (1989), *98–108.*
19. Pierański, Pi. Z. Kowalik, and M. Franaszek. Jumping particle model. a study of the phase space of a non-linear dynamical system below its transition to chaos. *J. Physique*, ***46*** (May, 1985), *681–686.*
20. Raibert, M. *Legged robots that balance*. MIT Press, Cambridge, MA, 1986.
21. Rizzi, A. and D. Koditschek. Progress in spatial robot juggling. In *Proceedings of the 1992 IEEE International Conference on Robotics and Automation*, 1992.
22. Routh, E. *Dynamics of a system of rigid bodies*. Dover, New York, 1905.
23. Schaal, S. and C. G. Atkeson. Open loop stable control strategies for robot juggling. In *IEEE Int. Conf. Rob. Aut.*, ***3***, Atlanta, May, 1993, pp. 913–918.
24. Schaal, S. D. Sternad, and C. G. Atkeson. *One-handed juggling: Dynamical solutions to a rhythmic movement task*. 1994.
25. Shirai, M. and A. Saito. Parts supply in Sony's general-purpose assembly system "smart". *Japan Journal of Advanced Automation Technology*, ***1***, (1989), 108–111.
26. Singer, N. C. and W. P. Seering. Utilizing dynamic stability to orient parts. *ASME Journal of Applied Mechanics*, ***54***, (December, 1987), 961–966.
27. Snavely, G. Personal communication, September, 1993. (Robotics Group Engineer, General Motors Tech Center).
28. Tufillaro, N. T. Abbott, and J. Reilly. *An experimental approach to nonlinear dynamics and chaos*. Addison-Wesley Publishing, Redwood City, CA, 1992.
29. Tufillaro, N. T. Mello, Y. Choi, and A. Albano. Period doubling boundaries of a bouncing ball. *J. Physique*, ***47*** (September, 1986), *1477–1482.*
30. Vakakis, A. F. and J. W. Burdick. Chaotic motions of a simplified hopping robot. In *Proc. IEEE Conference on Robotics and Automation*, IEEE, Cincinnati, 1990, pp. 1464–1469.
31. Wang, Y. *Dynamic analysis and simulation of mechanical systems with intermittent constraints*. Ph.D. dissertation, Carnegie Mellon University, 1989.
32. Wang, Y. and M. Mason. Two-dimensional rigid-body collisions with friction. *ASME Journal of Applied Mechanics*, ***59*** (September, 1992), *635–642.*
33. Wiegley, J. A. Rao, and K. Goldberg. Computing a statistical distribution of stable poses for a polyhedron. In *30th Annual Allerton Conference on Communications, Control and Computing*, University of Illinois, September, 1992, pp. 836–843.
34. Wiesenfeld, K. and N. Tufillaro. Suppression of period doubling in the dynamics of a bouncing ball. *Physica*, ***26D*** (1987), *321–335.*
35. Zumel, N. and M. Erdmann. Balancing of a planar bouncing object. In *IEEE International Conference on Robotics and Automation*, May 1994, pp. 2949–2954.

APPENDIX A. MAXIMAL AND SUPREMAL POINTS

A.1. Maximum Sustainable Energy

Since the robot-table has a maximum velocity $\dot{\rho}_0$, it can impart a limited amount of energy to the ball's motion. Using (2) and substituting $\dot{\chi} = \dot{\beta} - \dot{p}$, we obtain

$$\dot{\beta}' = -\dot{\rho}' = -\alpha\,(\dot{\beta} - \dot{\rho})$$

Under the high-mass robot-table assumption $\dot{\rho}' = \dot{\rho}$, and rearranging:

$$\dot{\beta}' = -\alpha\dot{\beta} + (1 + \alpha)\dot{\rho}$$

Note that if we assume $\dot{\rho} = 0$ (a stationary robot-table), each successive impact causes a loss of $(1 - \alpha)$ of the ball-part velocity. To sustain a given ball-part velocity, the robot-table must contribute this much velocity in the restitution equation. Seeking to maximize $\dot{\beta}'$ (and hence energy), we assume $\dot{\rho}$ to be its maximum of $\dot{\rho}_0$. Since we need sustainable $\dot{\beta}'$, we assume the equilibrium velocity $\dot{\beta}_{eq} = -\dot{\beta} = \dot{\beta}'$. Then,

$$(1 - \alpha)\dot{\beta}_{eq} = (1 + \alpha)\dot{\rho}_0$$

which leads directly to

$$\dot{\beta}_{eq} = \left(\frac{1+\alpha}{1-\alpha}\right)\dot{\rho}_0 \tag{33}$$

Noting that $\dot{\rho}_0$ can only occur when $\tau_c = 0$ and $\rho = 0$, it must be the case that $\beta = 0$ and $\dot{\beta} = \dot{\bar{\beta}}$, thus

$$E_{max} = \frac{1}{2}\left(\frac{1+\alpha}{1-\alpha}\,\dot{\rho}_0\right)^2 \tag{34}$$

A.2. Maximum Energy Change

As discussed in section 4, most of $\mathcal{H}$ loses energy with impact, while a small region gains energy. As a consequence of restitution and limited robot-table velocity, an upper bound exists on the $\Delta_1 E$ function on $\mathcal{H}$.

Finding the gradient of $\Delta_1 E$:

$$D(\Delta_1 E) := \begin{bmatrix} \dfrac{\partial \Delta_1 E}{\partial \beta} \\ \\ \dfrac{\partial \Delta_1 E}{\partial \dot{\bar{\beta}}} \end{bmatrix}$$

$$\frac{\partial \Delta_1 E}{\partial \bar{\beta}} = -\alpha\gamma - \gamma \tag{35}$$

$$\frac{\partial \Delta_1 E}{\partial \dot{\bar{\beta}}} = -\alpha\gamma T - (1-\alpha^2)\dot{\bar{\beta}} - \alpha(\alpha-1)\dot{\rho}_0 \tag{36}$$

Since (35) is constant (meaning $\Delta_1 E$ is unbounded as a function of $\bar{\beta}$), we conclude that the maximum $\Delta_1 E$ on the $\mathcal{H}$ region must occur on the $\bar{\beta} = 0$ boundary. The Kuhn-Tucker conditions require

$$\frac{\partial \Delta_1 E}{\partial \dot{\bar{\beta}}} = 0$$

which leads to a maximum:

$$\Delta E_{max} = \frac{1}{2}\,\frac{1+\alpha}{1-\alpha}\,\dot{\rho}_0^2 \tag{37}$$

at

$$\bar{b} = \left(0, \frac{\alpha\dot{\rho}_0}{\alpha - 1}\right).$$

Since $\Delta E_{max} > \Delta_2 E$, the result holds for the entire $\mathcal{H}$ region.

A.3. Supremum ΔE on $\mathcal{H}$–$\mathcal{R}$

In this section, we derive the supremum ΔE on the $\mathcal{H} - \mathcal{R}$ region. This quantity is important for the proof of finite-time attraction to $\mathcal{R}$.

A.3.1. ΔE_{sup} *not on* $R(\bar{b}) = 0$. In order for a supremal state, $\bar{b}_s$, to exist on $R(\bar{b}) = 0$, it must satisfy

$$D_{\bar{\beta}}\,\Delta_1 E(\bar{b}_s) = \lambda D_{\bar{\beta}} R(\bar{b}_s)$$

$$D_{\dot{\bar{\beta}}}\,\Delta_1 E(\bar{b}_s) = \lambda D_{\dot{\bar{\beta}}} R(\bar{b}_s) \tag{38}$$

where

$$D_{\bar{\beta}} R(\bar{b}) = -\gamma \text{ and } D_{\dot{\bar{\beta}}} R(\bar{b}) = -\dot{\bar{\beta}}.$$

Recalling from (35),

$$D_{\bar{\beta}} \Delta_1 E = -\alpha\gamma - \gamma,$$

which requires $\lambda = \alpha + 1$. Recalling from (36),

$$D_{\dot{\bar{\beta}}}\Delta_1 E = -\alpha\gamma T - (1-\alpha^2)\dot{\bar{\beta}} - \alpha(\alpha-1)\dot{\rho}_0,$$

and $\lambda = \alpha + 1$ does not satisfy (38). Thus, ΔE_{sup} cannot exist on $R(\bar{b}) = 0$.

A.3.2. Finding ΔE_{sup}. We then consider the leftmost boundary of $\mathcal{B}_1 - \mathcal{R}$ given by the line $\bar{\beta} = 0$. Noting that $\alpha^2 - 1 < 0$ for realistic α ($0 \leq \alpha < 1$), $\Delta_1 E$ must achieve its supremum where the curve, $R(\bar{b}) = 0$, intersects the line, $\bar{\beta} = 0$. This occurs at the state

$$\bar{\beta} = 0$$

$$\dot{\bar{\beta}} = -\sqrt{2(1+\alpha)}\,\frac{\dot{\rho}_0}{1-\alpha} \tag{39}$$

Recalling the definition of $\Delta_1 E$ from (16) and noting that (39) implies $\tau_c = 0$,

$$\begin{aligned}
\Delta E_{sup} &:= \Delta_1 E(\bar{b}_s) \\
&= \frac{1}{2}[-\alpha\,\dot{\bar{\beta}} + (1+\alpha)\dot{\rho}_0]^2 - \frac{1}{2}\dot{\bar{\beta}}^2 \\
&= \left[-\frac{1+\alpha}{1-\alpha} + 1 + \alpha - \sqrt{2(1+\alpha)}\,\frac{\alpha}{1-\alpha}\right] \times (1+\alpha)\dot{\rho}_0^2 \\
&< 0
\end{aligned}$$

We note that ΔE_{sup} is strictly negative, and that $\forall \bar{b} \in \mathcal{B}_1 - R$, $\Delta E(\bar{b}) < \Delta E_{sup}$.

A.4. Number of Impacts to Enter *R*

Next we find the supremum of $\Delta_1 E$ on the $\mathcal{B}_1 - \mathcal{R}$ region, ΔE_{sup}. Note that ΔE_{sup} is distinct from ΔE_{max}, as defined in (37). Recalling (35), the supremum of $\Delta_1 E$ must occur on the leftmost boundary of the $\mathcal{B}_1 - \mathcal{R}$ region. Because $\mathcal{B}_1 - \mathcal{R}$ is an open set, we first check the closure of the set defined by the boundary of $\mathcal{R}$, given by $R(\bar{b}) = 0$. Referring to Appendix section A.3.1, the supremum cannot exist on this boundary line. Referring to section A.3.2, we find ΔE_{sup} on the $\bar{b} = 0$ line and demonstrate that it is a strictly negative quantity.

Returning to the discussion of $\bar{b}_0$, we note that the ball-part will experience an energy change of at most ΔE_{sup} at each impact. The state of the ball-part will therefore enter $\mathcal{R}$ in at most $\left\lceil \dfrac{E(\bar{b}_0) - E_{max} - \Delta E_{max}}{-\Delta E_{sup}} \right\rceil$ impacts.

APPENDIX B. HANDY EQUATIONS, DEFINITIONS, AND PARAMETERIZATIONS

This appendix contains a brief summary of equations, definitions, and parameterizations which were useful in deriving our results. This summary is particularly useful when graphing simulation results, as in Figure 3.

B.1. Time to Collision

Time to collision, τ_c, is given by the solution of

$$\bar{\beta} + \dot{\bar{\beta}}\tau_c - \gamma\tau_c^2 = \dot{\rho}\tau_c - \gamma\tau_c^2$$

so that

$$\tau_c = \frac{\bar{\beta}}{\dot{\rho} - \dot{\bar{\beta}}},$$

assuming that the impact occurs within the first robot-table period.

Similarly, the robot-table period is given by the nonzero solution of

$$0 = \dot{\rho}T - \gamma T^2$$

so that

$$T = \frac{2\dot{\rho}_0}{\gamma}$$

B.2. Important Regions

The dynamics only have meaning when the ball-part is at or above the robot-table, so the possible states in the defined coordinates are limited to

$$\mathcal{H} := \{\bar{b} \mid \bar{\beta} \geq 0\}$$

$\mathcal{B}_1$ is defined as the region in which the ball-part impacts in less than one T. So:

$$\mathcal{B}_1 := \{\bar{b} \in \mathcal{H} \mid \tau_c < T\}$$

$\mathcal{B}_2$ is defined as the region in which the ball-part impacts in at least one T.

$$\mathcal{B}_2 := \{\bar{b} \in \mathcal{H} \mid \tau_c \geq T\}$$

The boundary line between $\mathcal{B}_1$ and $\mathcal{B}_2$ is then

$$\partial\mathcal{B}_2 := \{\bar{b} \in \mathcal{H} \mid \tau_c = T\}.$$

This line can be parameterized as

$$\dot{\bar{\beta}} = \begin{bmatrix} 1 \\ \\ -\dfrac{1}{T} \end{bmatrix} \bar{\beta} + r_0, \qquad \beta \geq 0.$$

B.3. System Dynamics

The system dynamics on β_1 are

$$\begin{aligned} \bar{f}_1(\bar{b}_k) &:= \alpha A_T \bar{b}_k + (\alpha - 1) A_{-\xi 1} r_0 \\ &= \bar{b}_{k+1} \\ A_t &:= \begin{bmatrix} 1 & t \\ 0 & 1 \end{bmatrix} \\ \xi_1 &:= \frac{\alpha T}{1-\alpha}. \end{aligned} \tag{41}$$

The dynamics on β_2 are

$$\bar{f}_1(\bar{b}_k) := -A_T x - \alpha_T$$

$$\alpha_T := \gamma T \begin{bmatrix} T/2 \\ \\ 1 \end{bmatrix}.$$

So that

$$\bar{f} := \begin{cases} \bar{f}_1 & : \bar{b} \in \beta_1 \\ \bar{f}_2 & : \bar{b} \in \beta_2 \end{cases}.$$

B.4. Fixed Point

The fixed point, e_1, of $\bar{f}_1$ is located at

$$e_1 = \begin{bmatrix} \dfrac{4\alpha\dot{\rho}_0^2}{(1+\alpha)^2\gamma} \\ \\ \dfrac{-1(1-\alpha)\dot{\rho}_0}{1+\alpha} \end{bmatrix}$$

B.5. Zero Energy Change Boundary

The zero energy change boundary, $\mathcal{B}_1^0$, is defined parametrically as

$$\mathcal{B}_1^0 := \left\{ \bar{b} \in \mathcal{H} \mid \dot{\bar{\beta}} = \gamma\tau_c - \frac{1+\alpha}{1-\alpha}(\dot{\rho}_0 - \gamma\tau_c) \right\}$$

B.6. Boundary of $\mathcal{R}$

The boundary of the attracting energy region, $\mathcal{R}$, is defined by

$$R(\bar{b}) = 0$$

where

$$\begin{aligned} R(\bar{b}) &:= E_{max} + \Delta E_{max} - E(\bar{b}) \\ &= \frac{1+\alpha}{(1-\alpha)^2}\dot{\rho}_0^2 - \gamma\bar{\beta} - \frac{1}{2}\dot{\bar{\beta}}^2. \end{aligned}$$

B.7. Table of Notation

Common notation is shown in Table II.

Table II Table of Notation

Symbol	*Explanation*
	Constants
γ	gravitational constant
α	coefficient of restitution
T	robot-table oscillation period $T := 2\dot{\rho}_0/\gamma$
$\dot{\rho}_0$	robot-table initial velocity
	Variables
t	time
τ_p	time elapsed since last minimum of ρ
r	state of robot-table $(\rho, \dot{\rho})$
ρ	position of robot-table
$\dot{\rho}$	velocity of robot-table
b	$(\beta, \dot{\beta})$ State of ball-part
β	position of ball-part
$\dot{\beta}$	velocity of ball-part
$\bar{b}$	$(\bar{\beta}, \dot{\beta})$ State of ball-part sampled at $\tau_p = 0$
$\bar{\beta}$	position of ball-part sampled at $\tau_p = 0$
$\dot{\bar{\beta}}$	velocity of ball-part sampled at $\tau_p = 0$

Table II Table of Notation (Continued)

Symbol	*Explanation*
	Functions
$F'(x)$	function describing trajectory of point with initial condition x flying in gravity for time t
$C_y(x)$	function describing instantaneous change of ball-part state y caused by impact with robot-table state x
$f(\bar{b}_k)$	discrete time function which specifies $(\bar{b}_{k+1})$
$\tau_c(\bar{\beta}, \dot{\bar{\beta}})$	Time to collision from time since start of period
$-\tau_c(\bar{\beta}, \dot{\bar{\beta}})$	Time until next period $(-\tau_c = T - \tau_c)$
A_t	used in flight calculations and recursions: $A_t := \begin{bmatrix} 1 & t \\ 0 & 1 \end{bmatrix}$
E	total energy of a given point: $E(\bar{b}) := \gamma \bar{\beta} + \frac{1}{2} \dot{\bar{\beta}}^2$
ΔE	change in energy at impact: $\Delta E(b) := E(f(b)) - E(b)$
K	kinetic energy of a given point: $K(\bar{b}) := \frac{1}{2} \dot{\bar{\beta}}^2$
	Regions
$\mathcal{H}$	The region of the b phase plane corresponding to physically realistic conditions
$\mathcal{B}_1$	The region in $\mathcal{H}$ for which $\tau_c < T$
$\mathcal{B}_2$	The region in $\mathcal{H}$ for which $\tau_c \geq T$
$\mathcal{R}$	The globally attracting total energy region
$\mathcal{K}$	The globally attracting kinetic energy region

Mathematical Problems in Engineering

Special Issue on
Short Range Phenomena: Modeling, Computational Aspects, and Applications

Call for Papers

In recent years, the mathematical formalism of impulsive systems (based on impulsive differential equations) has tried to join together the rigorous aspects from continuous systems formalism and the wide range of applications of discrete systems formalism. They were introduced to handle many evolution processes which are subject to singular short-term perturbations. Abrupt changes must be approached with mathematical and technical aspects dealing with the final evolution of such impulsive sources, whose effects are entirely transferred to the new state of the systems like transitions in quantum mechanics. Modern aspects in physics (quantum theory) and mathematics (wavelets, fractal theory) should be expedient in modeling short range phenomena and describing dynamics of perturbations and transitions in natural systems (advanced materials science) and advanced systems (optic, electronic, and quantum devices).

Thus, a special issue on all theoretical, computational, and practical aspects of modeling short range phenomena would be an opportunity of extending the research field of wavelets analysis, fractal theory, and applied mathematics (signal processing, control theory) for presenting new fundamental aspects in science and engineering. We are soliciting original high-quality research papers on topics of interest connected with modeling short range phenomena that include but are not limited to the following main topics:

- Mathematical aspects of pulse generation
- Dynamical and computational aspects of pulse measurement
- Wavelets analysis of localized space-time phenomena
- Stochastic aspects of pulses, sequences of pulses and time series

Authors should follow the Mathematical Problems in Engineering manuscript format described at the journal site http://www.hindawi.com/journals/mpe/. Prospective authors should submit an electronic copy of their complete manuscript through the journal's Manuscript Tracking System at http://mts.hindawi.com/, according to the following timetable:

Manuscript Due	June 1, 2008
First Round of Reviews	September 1, 2008
Publication Date	December 1, 2008

Guest Editors

Carlo Cattani, DiFarma, University of Salerno, Via Ponte Don Melillo, 84084 Fisciano (SA), Italy; ccattani@unisa.it

Ming Li, Department of Electronic Science & Technology, School of Information Science & Technology, East China Normal University, 3663 Zhongshan Bei Road, Shanghai 200062, China; mli@ee.ecnu.edu.cn

Cristian Toma, Faculty of Applied Sciences, Politehnica University, Hagi-Ghita 81, Bucharest Street 060032, Romania; cgtoma@physics.pub.ro